Acta Mechanica Sinica (2014) 30(3):447–456
DOI 10.1007/s10409-014-0044-7

RESEARCH PAPER

The impact of N-terminal phosphorylation on LHCII conformation in state transition

Jin-Hong Ding · Ning Li · Man-Liu Wang · Yan Zhang · Shou-Qin Lü · Mian Long

Received: 9 September 2013 / Revised: 5 November 2013 / Accepted: 22 November 2013

Abstract State transition is an important protection mechanism of plants for maintaining optimal efficiency through redistributing unbalanced excitation energy between photosystem II (PSII) and photosystem I (PSI). This process depends on the reversible phosphorylation/dephosphorylation of the major light-harvesting complex II (LHCII) and its bi-directional migration between PSII and PSI. But it remains unclear how phosphorylation/dephosphorylation modulates the LHCII conformation and further regulates its reversible migration. Here molecular dynamics simulations (MDS) were employed to elucidate the impact of phosphorylation on LHCII conformation. The results indicated that N-terminal phosphorylation loosened LHCII trimer with decreased hydrogen bond (H-bond) interactions and extended the distances between neighboring monomers, which stemmed from the conformational adjustment of each monomer itself. Global conformational change of LHCII monomer started from its stromal N-terminal (including the phosphorylation sites) by enhancing its interaction to lipid membrane and by adjusting the interaction network with surrounded inter-monomer and intra-monomer transmembrane helixes of *B*, *C*, and *A*, and finally triggered the reorientation of transmembrane helixes and transferred the conformational change to luminal side helixes and loops. These results further our understanding in molecular mechanism of LHCII migration during state transition from the phosphorylation-induced microstructural feature of LHCII.

Keywords State transition · LHCII · Phosphorylation · Conformation

1 Introduction

State transition is a short-term photosynthetic response of plants for acclimating to light environment changes and maintaining optimal efficiency through redistributing unbalanced excitation energy between photosystem II (PSII) and photosystem I (PSI) on the thylakoid membrane [1–5]. This regulation process depends on the reversible migration of the major light-harvesting complex II (LHCII) between PSII and PSI, the migration from PSII to PSI means dissociation of LHCII from PSII and bind to PSI, and the migration from PSI to PSII means the reverse process, i.e., the dissociation and rebinding of LHCII to PSII or PSI. PSII lighting that prefers PSII exciting initiates the migration of LHCII to PSI (state 1–state 2 transition) and PSI lighting that favors PSI exciting induces its backward migration to PSII (state 2–state 1 transition), by which the antenna cross section of the rate-limiting photosystem is adjusted and the excitation energy is redistributed [6]. Reversible phosphorylation/dephosphorylation, meaning the addition of a phosphate (PO_4^{3-}) group to a protein or reverse process, of LHCII initiated by the thylakoid-associated kinase STN7 activation/inactivation under PSII/PSI lighting is required for its forwards and backwards migration during state 1–state 2/state 2–state 1 transitions [7]. Two main models, surface charge model and molecular recognition model, have been proposed to explain the migration mechanism of LHCII. The

The project was supported by the National Key Basic Research Foundation of China (2006CB910303 and 2011CB710904), the National Natural Science Foundation of China (11072251 and 31230027), the CAS Knowledge Innovation Program (KJCX2-YW-L08), and the Scientific Research Equipment Project (Y2010030).

J.-H. Ding · N. Li · M.-L. Wang · Y. Zhang · S.-Q. Lü (✉1) · M. Long (✉2)
Key Laboratory of Microgravity
(National Microgravity Laboratory)
and Center of Biomechanics and Bioengineering,
Institute of Mechanics,
Chinese Academy of Sciences, 100190 Beijing, China
e-mail1: lsq@imech.ac.cn
e-mail2: mlong@imech.ac.cn

former proposes that LHCII phosphorylation results in structural changes of thylakoid membrane, and therefore initiate the lateral diffusion of LHCII or the spillover of excitation energy from PSII to PSI [8, 9]. The latter suggests that the phosphorylated LHCII exhibits different binding specificity for both photosystems in that the phosphorylation of the LHCII decreases its affinity to PSII and increases its affinity to PSI at the specific docking site through the conformational change of LHCII itself [2, 10]. Also the assembly manner of LHCII in the migration process remains controversial among monomer [11], trimer [12], and aggregates [13]. Thus, the impact of LHCII phosphorylation on structural change is an important issue for understanding the molecular mechanism of LHCII migration during state transition.

The basic structural and functional unit of LHCII is the trimer. Each monomer comprises one ~ 232 amino acid polypeptide [14], fourteen compactly bound chlorophylls (chls) in two varieties (*a* and *b*), four carotenoids in three different kinds, and two different types of lipids [15]. The secondary structure of monomeric LHCII polypeptide folds into three membrane-spanning helices of *B*, *C*, and *A*, two short helices of *E* and *D* on the luminal side, and four flexible loops on the stromal and luminal sides (cf., Fig. 1a). Chls distribution to the respective stromal and luminal surfaces directs the collection and transmission path of energy from luminal to stromal chls and further to the neighboring LHCIIs or photosynthetic reaction centers [16–18]. Spectroscopic studies indicate that LHCII phosphorylation induce a conformational change of its N-terminal domain, which leads to the disassembly of LHCII trimers into monomers [11]. However, the direct micro-structural evidences of how the LHCII phosphorylation regulates its conformation are still missing.

Here we applied molecular dynamics simulations (MDS) to elucidate the structural variations of pea LHCII trimer induced by its N-terminal phosphorylation. Conformational dynamics between phosphorylated and non-phosphorylated LHCII at atomic-level were compared. Key residues in different regions and their interactions were analyzed and the potential pathway of molecular allostery was proposed. These results would further our understanding in the molecular mechanism of LHCII migration during state transition.

2 Method

The crystallized LHCII trimer of pea (PDB code: 2BHW [17]) was employed with isolated polypeptides only. The N-terminal 1-9 amino acids which are absent in the crystallized structure were added by homology modeling using I-TASSER server for yielding the full-length structure of LHCII trimer [19]. Based on the potential phosphorylation sites of 3S and 5T [20], three simulation systems were built for evaluating the impact of phosphorylation on the LHCII conformation, as shown in Table 1. The first was the control system without phosphorylation (0P), i.e., no addition of phosphate (PO_4^{3-}) group to LHCII. The second was the one with only 5T residue being phosphorylated (1P), and the last was the one with both 3S and 5T residues being phosphorylated (2P), i.e., one phosphate (PO_4^{3-}) group was added to 5T residue in 1P system, and both 3S and 5T residues were added by phosphate (PO_4^{3-}) group in 2P system.

Table 1 Summary of simulation set-up

Systems	Description	Equilibration
		time × runs
0P	No phosphorylated LHCII trimer	50 ns × 3
1P	5T phosphorylated for all three monomers	50 ns × 3
2P	Both 3S and 5T phosphorylated for all three monomers	50 ns × 3

Each system was built by embedding the target LHCII trimer into a 60 Å × 60 Å (1 Å = 0.1 nm) rectangular POPE lipid membrane plate with 20 Å water layers capping each side of membrane, and then neutralized with ~ 100 mM Na^+ and Cl^- ions to mimic the physiological ionic environment (Figs. 1b and 1c). NAMD program [21] with CHARMM27 all-atom force field [22] were used for all simulations with an integration time step of 1 fs and the periodic boundary conditions. A smooth (10–12 Å) cutoff and the particle mesh ewald (PME) method were employed to calculate van der Waals forces and electrostatic interactions, respectively. Every simulation was started from energy minimization with gradually relieving of constraints, which included 10 000 steps with all components fixed except for those lipid membrane phosphorus atoms constrained along the *Z*-axis, followed by 10 000 steps with capping waters and neutralized ions being released, and, finally, 10 000 steps with only protein backbone and *Z*-axis of lipid phosphorus atoms being constrained. System heating was then performed from 0 to 300 K at 30 K increment every 5 ps. Finally, 50 ns free equilibration simulation was carried out after sequent 200 ps relaxation with both protein backbone and *Z*-axis of lipid phosphorus atoms being constrained and 300 ps relaxation with only protein backbone being constrained. The 300 K heat bath was manipulated by Langevin thermostat, and the 1 atm (1 atm = 1.01×10^5 Pa) pressure was controlled by Nosé-Hoover Langevin piston method during equilibration simulations. Each system was simulated three times independently (Table 1), in which each run exhibited stable conformation with slight fluctuations in the last 10 ns (see suplementary material Fig. S1).

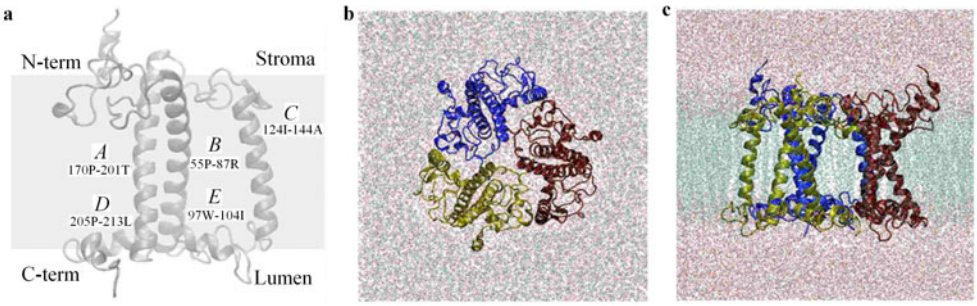

Fig. 1 LHCII structure and simulation system built-up. **a** Conformational features of LHCII monomer were illustrated with three long transmembrane helixes of *B* (55P-87R), *C* (124I-144A), and *A* (170P-201T) and two short helixes of *E* (97W-104I) and *D* (205P-213L) locating in luminal side as well as stromal and luminal peptides. The labeling of main helixes in this work followed the naming of pea LHCII crystal structures. **b**, **c** Schematic components of simulation systems under top view from stromal side **b** and side view **c**. The LHCII polypeptide were presented as newcartoon with different color for each monomer, and the surrounding lipid membrane and the capping water were both presented as name lines

The conformational features of LHCII were figured out mainly on the entire trimer and each monomer itself for evaluating the inter-monomer and intra-monomer changes, respectively. The former was quantified by the hydrogen bond (H-bond) interactions and the distances between monomer pairs. The latter was characterized by calculating the root of mean standard deviation (RMSD) of each residue or special fragments, the strength or occurrence frequency of H-bond interactions between target regions or between LHCII peptide and lipid membrane, and the orientation of transmembrane helixes *B*, *C*, and *A* which was defined by the angle between respective helix axis and *Z*-axis. The H-bond interaction was defined with a donor-acceptor distance < 3.5 Å and a donor-hydrogen-acceptor angle $< 45°$. The system built-up and data analysis were performed using VMD program [23].

3 Results

3.1 Inter-monomeric conformational changes of LHCII upon phosphorylation

Conformational state of LHCII trimer, a basic structural unit, plays a key role on its biological function. Here the inter-monomeric conformational changes upon phosphorylation were evaluated. The H-bond analysis indicated that the interactions between two neighboring monomers (black bars) mainly resulted from the interactions between neighboring stromal peptides (dark gray bars) and, especially, between luminal peptides (light gray bars) of different monomers, where those interactions between transmembrane helixes were negligible (Fig. 2a). N-terminal phosphorylation reduced the inter-monomeric interactions with decreased H-bond number from (8.2 ± 1.8) of 0P to (5.5 ± 1.5) of 1P or (6.8 ± 1.5) of 2P systems (black bars). The reduction arose from the weakening of luminal peptides interaction (light gray bars) but not of stromal peptides (dark gray bars) (Fig. 2a). Accordingly, the lessened inter-monomeric interaction due to the residue phosphorylation resulted in the increased distance between the backbone geometry centers of transmembrane helixes *B*, *C*, and *A* of any two of neighbor monomers (left bars), together with more remarkable increase on its luminal side (right bars) but almost constant on its stromal side (middle bars) (Figs. 2b and 2c). Moreover,

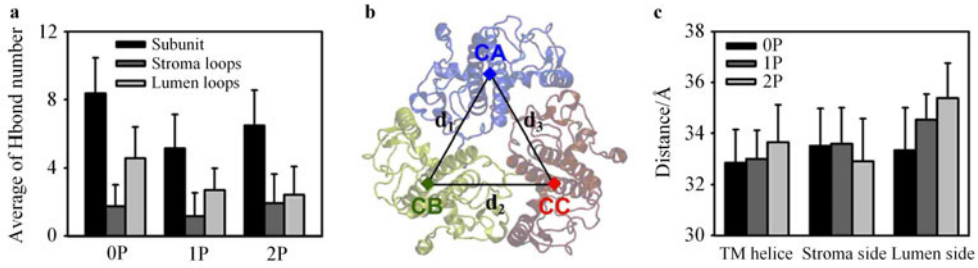

Fig. 2 Inter-monomeric changes of LHCII trimer upon phosphorylation. **a** Inter-monomeric H-bond interactions between whole subunits (black), stromal loops (dark gray) (1R-54D and 145G-169D), and luminal peptides (light gray) (87R-123S and 202G-232K) for non-phosphorylated (0P) (left), 5T phosphorylated (1P) (middle), and both 3S and 5T phosphorylated (2P) (right) systems. **b** Schematic definition of the inter-monomeric distance between the geometry centers of target peptide backbones. **c** Comparisons of the inter-monomeric distances between the backbone geometry centers of three transmembrane helixes (*B*: 55P-87R; *C*: 124I-144A; and *A*: 170P-201T) (left), stromal ends of three transmembrane helixes (57T-62R, 137A-142R and 172A-177K) (middle) and luminal ends of three transmembrane helixes (80V-85L, 126A-131Q and 194F-199I) (right) among 0P (black), 1P (dark gray) and 2P (gray) systems. The data were the average of three monomer pairs over the last 5 ns equilibration process for three independent runs ± *SD*

the more the occurring phosphorylation, the larger the distance (dark and light grey bars in Fig. 2c). Thus, the differences in the H-bond number and the center distance between 0P and 1P or 2P systems, even not so significant, implied that N-terminal phosphorylation reduced inter-monomeric interactions with enhanced inter-monomeric distances, which mainly resulted from the conformational change of luminal side.

3.2 Intra-monomeric conformational changes of LHCII upon phosphorylation

To further test if the conformational change of LHCII trimer results from the local structural variation of each monomer itself, the RMSD profiles for each residue of LHCII monomer were analyzed based on the backbone alignment of individual residue (Fig. 3a) or those of transmembrane helixes *B*, *C*, and *A* (Fig. 3b). The former representes the conformation of each residue itself, and the latter demonstrates the conformation of whole monomer. It was indicated that, for each monomer of 0P, 1P, and 2P systems, the RMSD value of single individual residues was low (< 0.2 Å) and stable in the regions of three long transmembrane helixes (helix *B*: 55P-87R; helix *C*: 124I-144A; helix *A*: 170P-201T) and two short luminal side helixes (helix *E*: 97W-104I; helix *D*: 205P-213L), but highly fluctuated with large and varied values in the other regions (Fig. 3a), which exhibited similar features of rigid core with flexible terminus studied using electron paramagnetic resonance [24]. Specifically, non-phosphorylated 0P system yielded larger fluctuations over the flexible regions than those of phosphorylated 1P and 2P systems. For example, just right after the phosphorylated site 5T, the RMSD values for the residues 6T-8K were smaller than 0.4 Å for 0P system but larger than 0.2 Å for both 1P and 2P systems (Fig. 3a).

To further elucidate the conformational landscape of whole monomer, RMSD profile was analyzed based on the backbone alignment of monomer transmembrane helixes. As shown in Fig. 3b, the results exhibited trend similar to that of the profile based on individual residue alignment, that is, it presented a relatively higher fluctuation for 0P system than those of 1P and 2P systems. By contrast, some distinct features were still found: firstly, the stability and consistency of the helix regions were abated with more ambiguous boundaries, which enlarged the conformational difference among 0P, 1P, and 2P systems; secondly, the difference between intact 0P and phosphorylated 1P or 2P system covered the entire regions from stromal N-terminal to luminal C-terminal (Fig. 3b). These results indicated that the residue phosphorylation resulted in noteworthy conformational change of LHCII monomer.

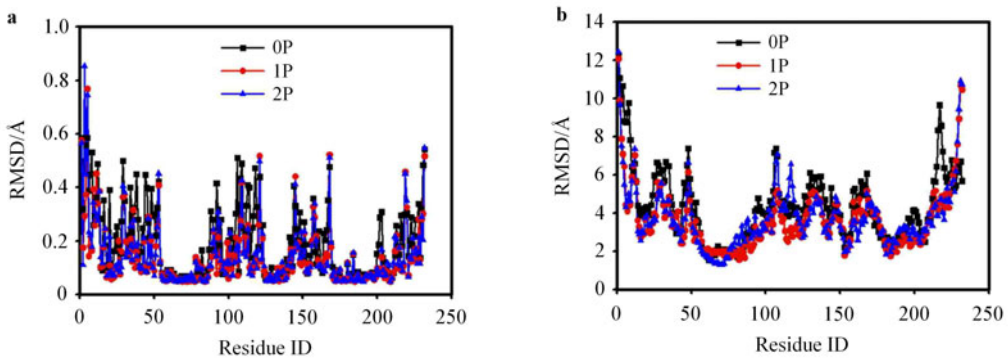

Fig. 3 Intra-monomeric conformational changes of LHCII upon phosphorylation. They were evaluated using the RMSD profiles of each residue upon single amino acid backbone alignment **a** and transmembrane helixes backbone alignment **b**. The data were presented as the average of three subunits over the last 5 ns equilibration process for three independent runs, and *SD*s were not shown for clarity

3.3 Key residue interactions to phosphorylation-induced conformational changes

Next, we should ask why and how the single- or double-residue phosphorylation of LHCII monomer would cause such the remarkable and global conformational change. It was reasonable to firstly focus on N-terminal (1R-54D) flexibility, since this peptide included the phosphorylation sites and served as the triggering source for further conformational regulation. Low RMSD values of N-terminal peptide in 1P and 2P, especially for the first 10 residues (Fig. 3b), indicated that the phosphorylation might form additional interactions to refine its flexibility. Our analysis demonstrated that more H-bonds strengthened the interactions between N-terminal peptide and lipid membrane for phosphorylated 1P and 2P systems, as compared to the 0P system with less H-bonds (Fig. 4a). Specifically, the enhanced interactions mainly resulted from those of phosphorylated 5T of 1P or both 3S and 5T of 2P to lipid membrane (Fig. 4b), because the residue phosphorylation added negative charges to the side-chain of the two sites and allow them interacting more effectively with the positively-charged head of lipid membrane.

By contrast, the interactions between N-terminal peptide and other parts of LHCII trimer did not show significant

difference in the presence or absence of N-terminal phosphorylation. Only the phosphorylation-induced variation was the reallocation of the major sites involved in the interactions. For example, the 47D and 50G sites were found to be the main residues for binding to the neighboring monomers in 0P system, but only 47D was reserved in 1P system and 47D, 31E, and 34S were dominated in 2P system (Fig. 4c and supplementary material Table S1), implying that the phosphorylation of specific residues (3S and 5T) modifies the H-bond interactions of other residues in one monomer with the other two monomers. And more residues were also involved in the interactions of N-terminal with other parts of autologous monomer (see supplementary material Table S2). N-terminal phosphorylation resulted in the further increase of dominant residues from three (43D, 52S, and 54D) for 0P system, to four (7K, 8K, 41P, and 54D) for 1P system, and five (8K, 41P, 44Y, 47D, and 54D) for 2P system. The 8K residue became the main binding site in the phosphorylated 1P and 2P systems (Fig. 4d). In short, LHCII N-terminal phosphorylation induced its conformational change, which resulted from the enhanced interaction with lipid membrane and the binding sites reallocation for inter-monomeric and intra-monomeric interactions.

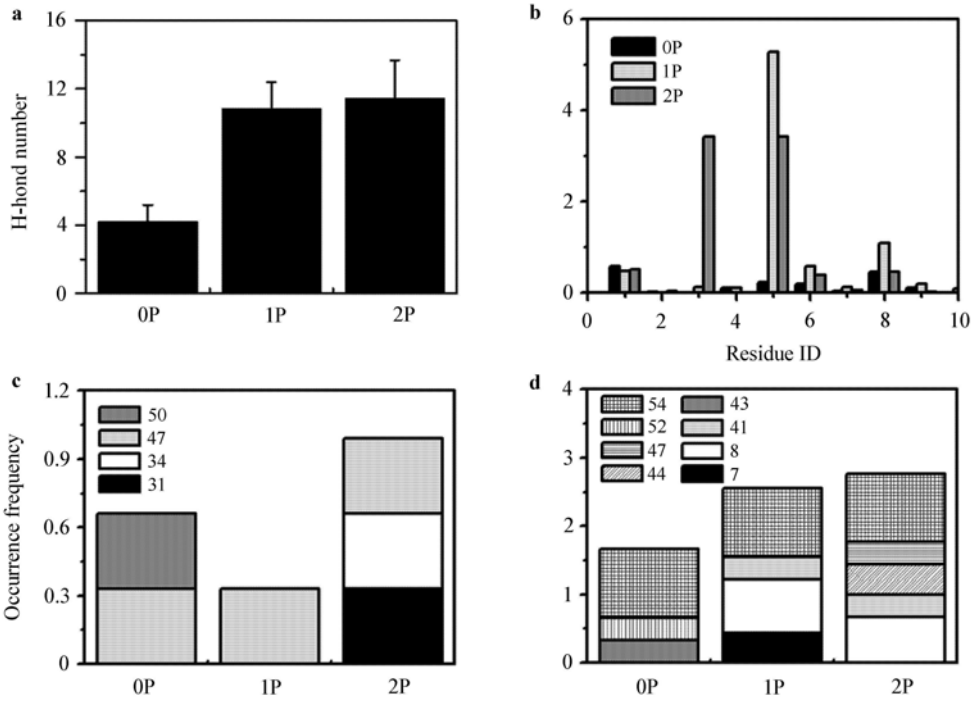

Fig. 4 Conformational changes of LHCII N-term (1R-54D) upon phosphorylation. The N-term–lipid membrane interactions were illustrated in **a** and **b** with the comparisons of all H-bonds **a** and corresponding distributions **b** among 0P, 1P, and 2P systems. The H-bond interactions were mainly concentrated in the phosphorylated residue sites of 5T or/and 3S, and for clarity, the first 10 residues were presented only. Data were presented as the average of three monomers over the last 5 ns equilibration process for three independent runs ($\pm SD$). The N-term–protein interactions were denoted in **c** and **d** with the comparisons of key residue distributions of N-term involving in the interactions to its neighbor subunits **c** and with other parts of the subunit self **d**. The data were presented as the occurrence frequency of the key residues, which was defined as the occurrence ratio of a residue involving in interactions for three monomers of three independent runs. Whether or not a residue had interactions was determined by if it keeps the stable H-bond interactions over the last 5 ns equilibration process. Only the residues with the frequencies of no less than 0.33 were shown for clarity

3.4 Conformational propagation of LHCII upon phosphorylation

Furthermore, how the N-terminal conformational change is propagated to the transmembrane helixes and luminal loops should be correlated intimately with corresponding structural features. Overall perspective of LHCII trimer exhibits that each monomeric N-terminal is surrounded by transmembrane *B* and *A* helixes from autologous monomer and *B* and *C* helixes from counterclockwise neighboring monomer (Fig. 5). A possible mechanism referred to that the conformational change of N-terminal upon phosphorylation triggered the change of its interaction with encircled transmembrane helixes from autologous or neighboring monomers, which induced the reorientation of transmembrane helixes and then forced the conformational change of luminal side loops.

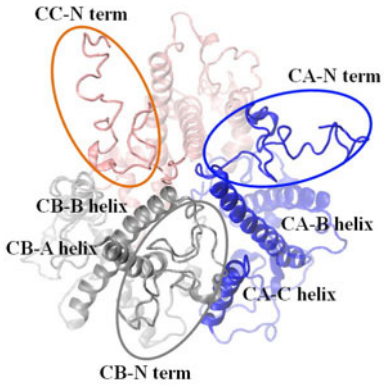

Fig. 5 Location features of LHCII N-terminal (1R-54D). LHCII trimer was presented as newcartoon with different colors of blue, silver, and pink for respective monomer from stromal side to luminal side (top view). Corresponding N-terminal structure for each monomer was highlighted with labeled ellipse of *CA*-N, *CB*-N, and *CC*-N-terms in short, respectively. Each N-terminal was surrounded by transmembrane helixes of *B* and *A* from autologous monomer, and by the helixes of *B* and *C* from its anticlockwise neighboring monomer. Only those helixes encircling N-terminal of monomer *CB*, named as "*CB-B* helix" and "*CB-A* helix" for terming the helixes *B* and *A* of monomer *CB*, or named as "*CA-B* helix" and "*CA-C* helix" for the helixes *B* and *C* of monomer *CA*, were labeled for the sake of clarity

To test this hypothesis, we firstly analyzed the distribution of main residues involved in the interactions of N-terminal and transmembrane helixes. On the one hand, the 61N residue of transmembrane *B* helix gradually released its interaction to autologous monomeric N-terminal. The occurrence frequency was reduced from 44% in 0P system to 33% and 11% in 1P and 2P systems, respectively (see supplementary material Table S3 and Fig. 6a1), suggesting that the N-terminal phosphorylation lowers the probability to reserve the interactions. And this interaction release offered more freedom of 61N side-chain for its rotation from pointing toward 52S in 0P system (Fig. 6a2) to gradual deviation in 1P (Fig. 6a3) and 2P (Fig. 6a4) systems. On the other hand, the 61N was also liberated gradually from clockwise neighboring monomeric N-terminal interaction with a reduced occurrence frequency of 44% in 0P system to 33% in 1P system and complete disappearance in 2P system (see supplementary material Table S5 and Fig. 6c1). Inversely, the 56E became more and more dominated since the frequency increased from zero in 0P to 33% in 1P and 67% in 2P systems (see supplementary material Table S5 and Fig. 6c1), due to the newly-formed H-bonds through re-orientating its negatively charged side-chain to 34S or 35Y in the phosphorylated 1P and 2P systems (Figs. 6c1–6c3). The release of 61N from autologous and neighboring N-terminal interaction and the new involvement of 56E for neighboring N-terminal binding cooperatively adjusted their side-chain orientation, which offered the potential driving force for the re-orientation of the entire transmembrane helix *B*.

By contrast, helix *A* regulated its interactions to the autologous N-terminal with increased occurrence frequency of 175E from 22% in 0P system to 78% and 56% in respective 1P and 2P systems, and with slightly decreased occurrence frequency of 185R from 44% in 0P system to 33% in 1P and 2P systems (see supplementary material Table S4 and Fig. 6b1). The residue of N-terminal for binding 175E transferred from 14S in 0P system to 8 K in both 1P and 2P systems (supplementary material Table S4). Similarly, the enhanced interaction of 175E and the readjustment of binding residues of N-terminal also changed its side-chain orientation (Figs. 6b2–6b4), which might provide a potential triggering force for the reorientation of the entire transmembrane helix *A*. Meanwhile, the interactions between N-terminal of each monomer and helix *C* of counterclockwise neighboring monomer were relatively weaker, since the H-bond analyses showed that only 147P was involved in 0P system with low occurrence frequency of 11%, and only 142R was involved in 2P system with occurrence frequency of 33% for binding the counterpart residue of 31E or 47D (see supplementary material Table S6 and Fig. 6d1). Corresponding conformations of the key residues were illustrated in Figs. 6d2–6d4. These results suggested that these residues of transmembrane helixes *B*, *C*, and *A* adjusted, by re-orientating their side-chains, their interactions to the autologous and/or neighboring phosphorylated N-terminal, which offered the possibility to drive the reorientation of corresponding entire helix and transfer the conformational change from stromal side to luminal side.

To further test the hypothesis, we quantified the orientation of helix *B*, *C*, or *A*, using the angle between the helix axis and *Z*-axis. The results indicated that the N-terminal phosphorylation enhanced the angle for helix *B* (Fig. 7a) but reduced it for helix *C* (Fig. 7d) and helix *A* (Fig. 7g). Moreover, the orientation changes of helixes *B* and *C* became more remarkable with the phosphorylation degree from 1P to 2P system (Figs. 7a and 7d). Intuitive comparison of helix orientation was respectively illustrated in Figs. 7b, 7e, and 7h for helix *B*, *C*, and *A*, demonstrating the significant conformational changes at the luminal and stromal surfaces. And side-chain orientations of key residues were positively correlated with whole helix orientations as shown in Fig. 7c, 7f and 7i for helixes *B*, *C*, and *A*, respectively, mapping these distinct key residues at the stromal surface for different helices. Thus, based on the conformational advantage of surrounding transmembrane helixes from autologous and neighboring monomers, the phosphorylated N-terminal triggered the reorientation of transmembrane helixes by affecting its H-bond interactions with the respective key residues.

3.5 Conformational change of LHCII luminal side upon phosphorylation

Reorientation of transmembrane helixes *B*, *C*, and *A* induced by N-terminal phosphorylation would certainly affect the conformations of luminal side, including the helix *E* be-

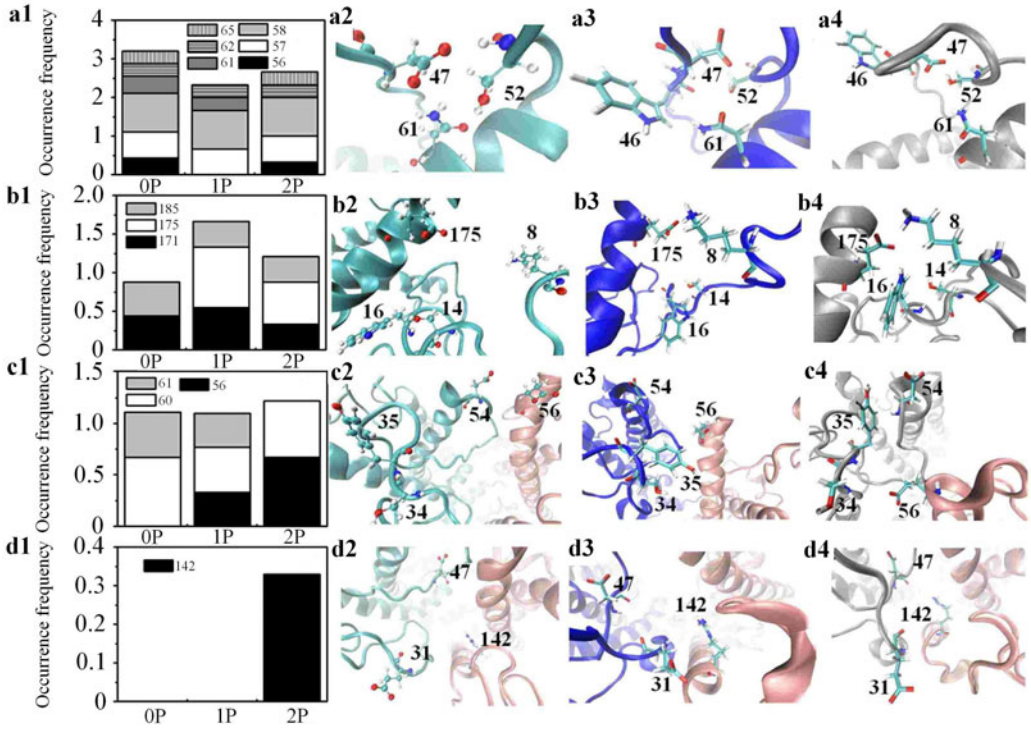

Fig. 6 Interaction network changes of transmembrane helixes of *B*, *C*, and *A* to LHCII N-terminal upon phosphorylation. Comparisons of the distribution (Figs. 6a1,6b1,6c1, and 6d1) and conformation (Figs. 6a2–6a4, 6b2–6b4, 6c2–6c4, 6d2–6d4,) of key residues from transmembrane helixes of *B*, *C*, and *A* which involved in H-bond interactions to N-terminal (1R-54D). Occurrence frequencies of key residues from self helix *B* (Fig. 6a1), self helix *A* (Fig. 6b1), counterclockwise neighboring helix *B* (Fig. 6c1) and helix *C* (Fig. 6d1) were compared among 0P (left), 1P (middle), and 2P (right) systems for evaluating the distributions of main residues involved in interactions to N-terminal. The definitions of occurrence frequency and interaction were the same as used in Fig. 4, and only the residues with the frequency of 0.33 or more were shown for the sake of clarity. Conformational comparison was done in Figs. 6a2–6a4 for autologous helix *B*, Figs. 6b2–6b4 for autologous helix *A*, Figs. 6c2–6c4 for counterclockwise neighboring helix *B* and Figs. 6d2–6d4 for counterclockwise neighboring helix *C*. Partial monomeric conformations were presented as cyan (0P), blue (1P), and silver (2P) newcartoon in Figs. 6a2–6a4, 6b2–6b4, 6c2–6c4, 6d2–6d4, and neighboring monomers were presented as pink newcartoon in Figs. 6c2–6c4 and 6d2–6d4. Key residues were termed with sequence number and demonstrated by name colored CPK, Licorice, and Bonds for 0P (Figs. 6a2, 6b2, 6c2, 6d2), 1P (Figs. 6a3, 6b3, 6c3, 6d3) and 2P (Figs. 6a4, 6b4, 6c4, 6d4), respectively. 50 ns snapshots of 0P run1, 1P run2 and 2P run1 were presented

tween helixes *B* and *C*, the helix *D* and C-terminal loop of LHCII right after helix *A*. Crystallized structure of LHCII trimer showed that the C-terminal loop of each monomer is almost parallel to helix *E* of counterclockwise neighboring monomer (Fig. 8b). Thus, we calculated the H-bond interactions between C-terminal peptide (214A–232K) and helix *E* to evaluate the conformational change of luminal side loop upon phosphorylation. The results indicated that the averaged H-bond number decreased gradually from 0P to 1P and to 2P system (Fig. 8a). The parallel nature between C-terminal peptide and helix *E* from neighboring monomers of 0P system (Fig. 8b) was disrupted gradually due to the lateral deviation and vertical crossing of C-terminal peptide in 1P (Fig. 8c) and 2P (Fig. 8d) systems. Also the interactions between luminal helix *D* and C-terminal peptide yielded remarkable difference with close location in 0P and distant separation in 1P and 2P systems (Figs. 8b–8d). In short, the reorientation of transmembrane helixes *B*, *C*, and *A* modulated the conformation of luminal helixes and loops, and finally promoted the conformational transfer from stromal side to luminal side.

4 Discussion

As an important antenna protein, LHCII plays key role in modulating the energy distribution between PSII and PSI. Although a few models of LHCII migration were proposed from phenomenological observations in plenty of experiments [2, 8, 25], the corresponding molecular mechanism seemed controversial since the micro-structural studies of LHCII migration upon phosphorylation were missing [11–13]. The goal of this work is to evaluate the conformational change of LHCII upon phosphorylation using MDS, and to further our micro-structural understandings in the molecular mechanism of LHCII migration during state transition. Our results indicated that the N-terminal phosphorylation loosened the LHCII trimer by reducing the H-bond interactions

and enlarged the distance between any two of monomers. Global conformational change of each monomer stemmed from stromal N-terminal, followed by the adjusted interaction network between N-terminal and its surrounding transmembrane helixes, and finally, transferred to luminal side via re-orientating these transmembrane helixes.

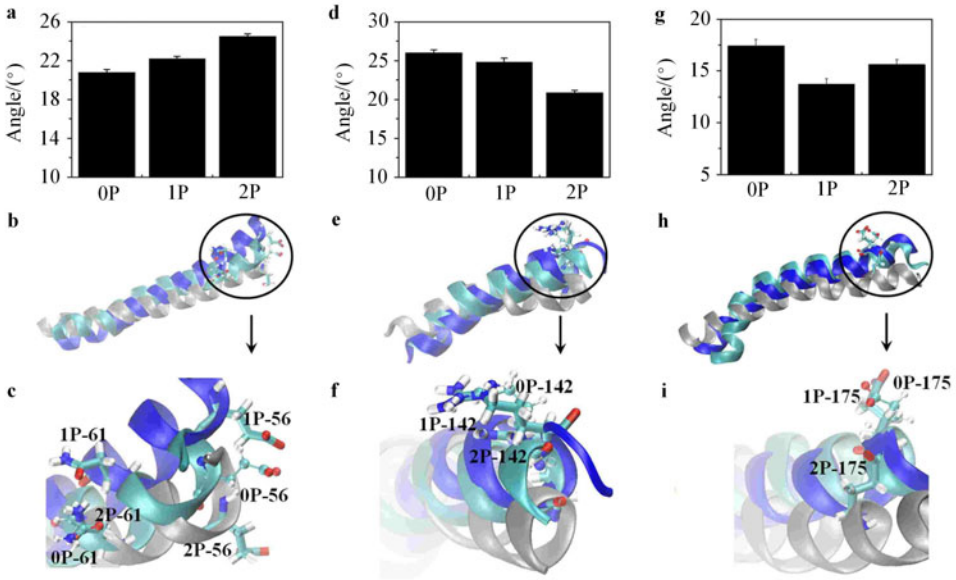

Fig. 7 Orientation changes of transmembrane helixes of *B*, *C*, and *A* upon phosphorylation. Orientations (Figs. 7a, 7d, and 7g), schematic reorientation (Figs. 7b, 7e, and 7h), and involved key residues (Figs. 7c, 7f, and 7i) were illustrated for helix *B* (Figs. 7a–7c), helix *C* (Figs. 7d–7f), and helix *A* (Figs. 7g–7i), respectively. The angle between helix *B* axis pointing from 55P to 87R, helix *C* axis pointing from 144A to 124I, or helix *A* axis pointing from 170P to 201T and *Z*-axis pointing from luminal to stromal side was used for determining their respective orientation. Data were presented as the average of three subunits over the last 5 ns equilibration process for three independent runs $\pm SD$. Only transmembrane helixes were presented as cyan, blue and silver newcartoon for 0P, 1P and 2P, respectively, based on backbone alignment of trimer transmembrane helixes. Key residues were demonstrated by name colored CPK, Licorice, and Bonds in Figs. 7c, 7f, and 7i for 0P, 1P, and 2P, respectively. 50 ns snapshots of 0P run1, 1P run2, and 2P run1 were presented

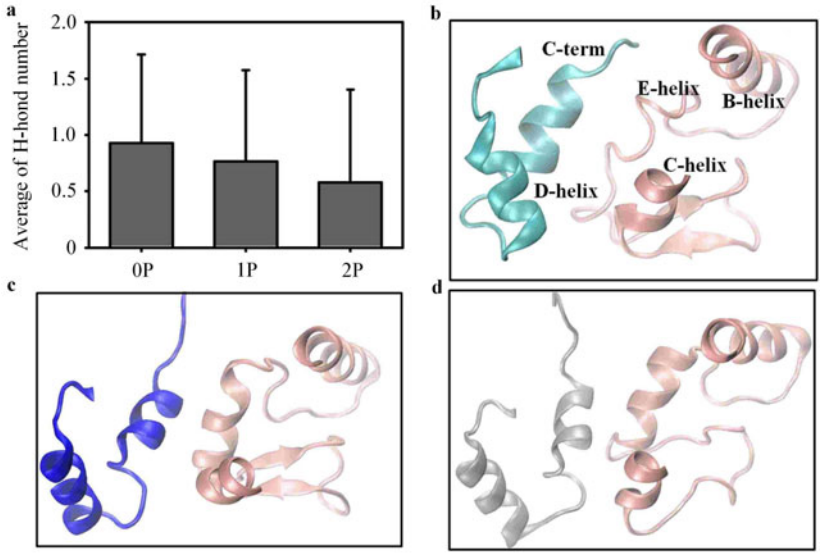

Fig. 8 Lumen inter-monomeric interaction changes between C-terminal (214A-232K) and helix *E* (97W-104I) upon phosphorylation. H-bond interactions were illustrated in **a** as the average $\pm SD$ of each monomer pairs over the last 5 ns equilibration process for three independent runs. Conformational charateristics were presented in *B*, *C*, and *D* for 0P, 1P, and 2P, respectively. 50 ns snapshots of 0P run1, 1P run2 and 2P run1 were presented with the same colors in Figs. 6 and 7

Main findings from our simulations are in good agreement with experimental studies. For example, the conformational feature of N-terminal peptide, especially three individual sections of 59S-26G, 26G-14S, and 14S-1R (Fig. 3), are dominated by flexible structure [24]. And the trimer loosing upon phosphorylation favors the spectroscopic suggestion of monomeric migration of LHCII [11]. The conformational change of luminal side loops is inclined to the molecular recognition model for LHCII migration, because this structural variation offers the possibility to adjust its binding affinity to the potential docking sites of PsaI/H/O subunits of PSI, which all located at luminal side [26–28]. Not only these comparisons impart confidence for our simulations, but they also provide a global and subtle conformational landscape of LHCII upon phosphorylation, which is still missing due to the limitation of experimental techniques.

From the structural evolution of LHCII trimer observed in the current work, we proposed a possible conformation allosteric pathway and mapped the key residues for modulating the conformational propagation. Basically, N-terminal phosphorylation at the site 3S and/or 5T favors the disassembly of LHCII trimer. N-terminal conformational change at the stromal side is able to propagate to the luminal side via reallocating the key residue interactions and re-orientating three transmembrane helices. Our simulations provide clues for regulating the state transition via altering the conformation of LHCII trimer, as well as for manifesting the roles of key residues in LHCII function via point mutagenesis.

MD simulation is an effective approach for structural analysis and has been widely applied to explore the dynamics of conformational evolution at atomic-level for predicting or validating the structure-function relationship of target proteins [29–31]. This approach would remedy the deficiency of experimental techniques and obtain a picture of dynamic, membrane-inserted, and phosphorylated LHCII with high-resolution. But the MD simulations still has some limitations in functional prediction for LHCII migration. In the current work, for example, the simulation systems were simplified by excluding the chlorophylls, carotenoids, and phosphatidylglycerols, mainly due to the limitation of missed force field parameters for the complicated pigments and phospholipids as well as the consideration of balancing computational costs and physiological representation. In fact, current viewpoint in the state transition prefers the regulation of absorption cross-section of two photosystems resulting from the reversible dissociation/association of LHCII between PSII and PSI. Whether the conformational change of LHCII peptide affects the energy absorption and transfer ability through modulating the location or linkage of pigments requires further studies. Nevertheless, this work offers clues for understanding the molecular mechanism of LHCII migration during state transitions.

Acknowledgement We thank Dr. Li-Xin Zhang from Institute of Botany, Chinese Academy of Sciences (CAS) for helpful discussion. MD simulations were performed on Supercomputing Center, CAS.

References

1 Allen, J.F.: Botany. State transitions—A question of balance. Science **299**, 1530–1532 (2003)

2 Allen, J.F., Forsberg, J.: Molecular recognition in thylakoid structure and function. Trends Plant Sci. **6**, 317–326 (2001)

3 Haldrup, A., Jensen, P.E., Lunde, C., et al.: Balance of power: a view of the mechanism of photosynthetic state transitions. Trends Plant Sci. **6**, 301–305 (2001)

4 Dietzel, L., Brautigam, K., Pfannschmidt, T.: Photosynthetic acclimation: State transitions and adjustment of photosystem stoichiometry-functional relationships between short-term and long-term light quality acclimation in plants. FEBS J. **275**, 1080–1088 (2008)

5 Kargul, J., Barber, J.: Photosynthetic acclimation: structural reorganisation of light harvesting antenna–role of redox-dependent phosphorylation of major and minor chlorophyll a/b binding proteins. FEBS J. **275**, 1056–1068 (2008)

6 Kouril, R., Zygadlo, A., Arteni, A.A., et al.: Structural characterization of a complex of photosystem I and light-harvesting complex II of Arabidopsis thaliana. Biochem. **44**, 10935–10940 (2005)

7 Bellafiore, S., Barneche, F., Peltier, G., et al.: State transitions and light adaptation require chloroplast thylakoid protein kinase STN7. Nature **433**, 892–895 (2005)

8 Barber, J.: Influence of surface charges on thylakoid structure and function. Annu. Rev. Plant Physiol. **33**, 261–295 (1982)

9 Georgakopulos, J.H., Argyroudi-Akoyunoglu, K.H.: On the question of the lateral migration of LHCII upon thylakoid protein phosphorylation in isolated pea chloroplasts: The stroma lamellar fraction separated from phosphorylated chloroplasts is not homogeneous. Biochim. Biophys. Acta **1188**, 380–390 (1994)

10 Wollman, F.A.: State transitions reveal the dynamics and flexibility of the photosynthetic apparatus. EMBO J **20**, 3623–3630 (2001)

11 Nilsson, A., Stys, D., Drakenberg, T., et al.: Phosphorylation controls the three-dimensional structure of plant light harvesting complex II. J. Biol. Chem. **272**, 18350–18357 (1997)

12 Dietzel, L., Brautigam, K., Steiner, S., et al.: Photosystem II supercomplex remodeling serves as an entry mechanism for state transitions in Arabidopsis. Plant Cell **23**, 2964–2977 (2011)

13 Minagawa, J.: State transitions–the molecular remodeling of photosynthetic supercomplexes that controls energy flow in the chloroplast. Biochim. Biophys. Acta **1807**, 897–905 (2011)

14 Standfuss, J., Kuhlbrandt, W.: The three isoforms of the light-harvesting complex II: Spectroscopic features, trimer formation, and functional roles. J. Biol. Chem. **279**, 36884–36891 (2004)

15 Rogl, H., Schodel, R., Lokstein, H., et al.: Assignment of spectral substructures to pigment-binding sites in higher plant light-harvesting complex LHC-II. Biochem. **41**, 2281–2287 (2002)

16 Kuhlbrandt, W., Wang, D.N., Fujiyoshi, Y.: Atomic model of plant light-harvesting complex by electron crystallography. Nature **367**, 614–621 (1994)

17 Standfuss, R., van Scheltinga, A.C.T., Lamborghini, M., et al.: Mechanisms of photoprotection and nonphotochemical quenching in pea light-harvesting complex at 2.5Å resolution. EMBO J. **24**, 919–928 (2005)

18 Liu, Z.F., Yan, H.C., Wang, K.B., et al.: Crystal structure of spinach major light-harvesting complex at 2.72 angstrom resolution. Nature **428**, 287–292 (2004)

19 Roy, A., Kucukural, A., Zhang, Y.: I-TASSER: A unified platform for automated protein structure and function prediction. Nat. Protoc. **5**, 725–738 (2010)

20 Michel, H., Bennett, J.: Use of synthetic peptides to study the substrate-specificity of a thylakoid protein-kinase. FEBS Lett. **254**, 165–170 (1989)

21 Phillips, J.C., Braun, R., Wang, W., et al.: Scalable molecular dynamics with NAMD. J. Comput. Chem. **26**, 1781–1802 (2005)

22 MacKerell, A.D., Bashford, D., Bellott, M., et al.: All-atom empirical potential for molecular modeling and dynamics studies of proteins. J. Phys. Chem. B **102**, 3586–3616 (1998)

23 Humphrey, W., Dalke, A., Schulten, K.: VMD: Visual molecular dynamics. J. Mol. Graph. **14**, 33–38 (1996)

24 Dockter, C., Muller, A.H., Dietz, C., et al.: Rigid core and flexible terminus: Structure of solubilized light-harvesting chlorophyll a/b complex (LHCII) measured by EPR. J. Biol. Chem. **287**, 2915–2925 (2011)

25 Allen, J.F.: How does protein phosphorylation regulate photosynthesis? Trends Biochem. Sci. **17**, 12–17 (1992)

26 Zhang, S., Scheller, H.V.: Light-harvesting complex II binds to several small subunits of photosystem I. J. Biol. Chem. **279**, 3180–3187 (2004)

27 Jensen, P.E., Haldrup, A., Zhang, S., et al.: The PSI-O subunit of plant photosystem I is involved in balancing the excitation pressure between the two photosystems. J. Biol. Chem. **279**, 24212–24217 (2004)

28 Lunde, C., Jensen, P.E., Haldrup, A., et al.: The PSI-H subunit of photosystem I is essential for state transitions in plant photosynthesis. Nature **408**, 613–615 (2000)

29 Mao, D.B., Lü, S.Q., Li, N., et al.: Conformational stability analyses of alpha subunit I domain of LFA-1 and Mac-1. PLoS One **6**, e24188 (2011)

30 Lü, S.Q., Zhang, Y., Long, M.: Visualization of allostery in P-selectin lectin domain using MD simulations. PLoS One **5**, e15417 (2010)

31 Zhang, M., Lü, S.Q., Li, G., et al.: Identification of a residue in helix 2 of rice plasma membrane intrinsic proteins that influences water permeability. J. Biol. Chem. **285**, 41982–41992 (2010)